Available online at www.sciencedirect.com
ScienceDirect
Journal of the European Ceramic Society 29 (2009) 1743–1753
www.elsevier.com/locate/jeurceramsoc

Anodically formed oxide films on niobium: Microstructural and electrical properties

H. Störmer [a,*], A. Weber [b], V. Fischer [b], E. Ivers-Tiffée [b], D. Gerthsen [a]

[a] *Laboratorium für Elektronenmikroskopie, Universität Karlsruhe, D-76128 Karlsruhe, Germany*
[b] *Institut für Werkstoffe der Elektrotechnik, Universität Karlsruhe, D-76128 Karlsruhe, Germany*

Received 18 July 2008; received in revised form 16 October 2008; accepted 24 October 2008
Available online 18 December 2008

Abstract

The electrical and structural properties of nanoscale niobium pentoxide (Nb_2O_5) dielectric layers in niobium-based solid electrolyte capacitors were studied. The Nb_2O_5 layers are formed by anodic oxidation of Nb-powder compacts. Capacitance measurements show a strong bias-voltage dependence of the capacitance after anodization. Heat treatments at temperatures up to 320 °C, which are applied in the capacitor-production process, lead to an increase of the capacitance and a reduction of the bias dependence. Based on the electrical and structural properties, which are characterized by electron microscopic techniques, a model is presented which explains the behavior of the specific capacitance after the various processing steps.

Keywords: Capacitor; Nb_2O_5; Electrical properties; Electron microscopy

1. Introduction

Surface mounted device (SMD) solid electrolyte tantalum capacitors play a major role in the passive components industry due to their high reliability, high volumetric efficiency and low equivalent series resistance.[1–5] Applications comprise for example buffer and smoothing capacitors in the power supplies of plug-in modules in computers. Solid electrolyte tantalum capacitors are fabricated on the basis of the tantalum/tantalum pentoxide (Ta_2O_5) system, where Ta_2O_5 dielectric layers are formed on porous metal powder compacts by anodic oxidation. The capacitance in these capacitor structures is given by $C = \varepsilon\varepsilon_0(A/d)$ with the permittivity of the dielectric ε, the vacuum permittivity ε_0, the overall area A and the thickness d of the dielectric layer. The proportionality of capacitance and area motivates efforts to increase the overall area A within a specific capacitor form, which makes it an objective to reduce the grain sizes of the powders for capacitor fabrication. Alternatively, higher specific capacitances can be also achieved by substitution of tantalum with $\varepsilon_{Ta2O5} = 27$ by a material system with allows the formation of a dielectric with higher permittivity. One logical substitute has always been the niobium/niobium pentoxide (Nb_2O_5) system with $\varepsilon_{Nb2O5} = 41$[6–8] which offers in addition the advantage of higher abundance and hence, lower raw material price, as well as similar behavior under anodization. Although the emergence of solid electrolyte niobium capacitors already started in the late sixties of the last century in the former Soviet Union, the lack of sophisticated niobium powders prevented a broader use of niobium capacitors on the world market at that time. However, in order to meet further demands, leading capacitor powder producing companies developed new processes in the meantime which now allow manufacture of capacitor-grade niobium and niobium-based metal powders which meet all requirements for capacitor fabrication.[9–14] As a consequence, major capacitor manufacturers launched production of niobium-based capacitors in 2001 which have the potential to replace tantalum in certain applications.[15–19]

One drawback of Nb-based capacitors which is often referred to in the literature is the pronounced temperature sensitivity of the Nb_2O_5 film.[20–23] Since the fabrication process of solid electrolyte capacitors with MnO_2 cathode comprises several production steps at elevated temperatures, the comprehensive understanding of the influence of heat treatments on the electrical properties of nanoscale Nb_2O_5 layers on niobium is essential.

* Corresponding author.
E-mail address: stoermer@lem.uni-karlsruhe.de (H. Störmer).

0955-2219/$ – see front matter © 2008 Elsevier Ltd. All rights reserved.
doi:10.1016/j.jeurceramsoc.2008.10.019

One possibility to overcome the thermally driven degradation of the dielectric oxide is doping the niobium powders.[24] For example, nitrogen or oxygen was added to the niobium powders in order to modify the oxygen diffusion kinetics, since oxygen diffusion from the dielectric layer into the metal substrate is thought to be one major reason for final capacitor failure. But in spite of these efforts in the fabrication of Nb-based solid electrolyte capacitors, a comprehensive understanding of the relations between processing parameters, microstructure development and resulting electrical properties is still not achieved. It is therefore the goal of the present work to clarify the correlation between heat treatment, microstructure development and electrical performance which is essential for the manufacture of niobium capacitors with stable electrical parameters. We present the results of a detailed characterization of anodically grown nanoscale Nb_2O_5 layers on niobium after anodization and subsequent thermal treatment. Impedance spectroscopy was applied for electrical characterization. Thermogravimetry yields information on the uptake of oxygen during annealing. Detailed microstructural characterization was performed using scanning (SEM) and transmission electron microscopy (TEM). Energy-filtered selected area electron diffraction (SAED) allows the evaluation of nearest neighbor distances within the amorphous dielectric oxide layer. A model will be presented which explains the behavior of the specific capacitance after anodization, annealing treatments at various temperatures and after a second anodization step.

2. Experimental procedures

2.1. Sample preparation

For sample preparation, pure niobium powders (*H.C. Starck Inc.*) as described in detail by Schnitter et al.[10] were used. Sample preparation followed the commercial capacitor fabrication process which involves uniaxial die pressing and sintering of capacitor-grade metal powder. During pressing, a tantalum wire was embedded into the green powder compact to ensure electrical contact. After vacuum sintering ($p = 10^{-4}$ Pa, 1260 °C), the metal powder compacts had a size of approximately $3 \times 1.5 \times 4\,mm^3$ and exhibited a porous, sponge-like microstructure. In order to form the amorphous nanoscale dielectric layer, the well established manufacturing process of commercial SMD (surface mounted device) tantalum capacitors which is based on a two-stage anodic oxidation (galvanostatic and potentiostatic) in an electrolyte solution was applied. All samples investigated in this study were anodized using 1 wt% aqueous solution of phosphoric acid (65 °C) employing an anodization voltage of 40 V and a maximum current density of 150 mA/g since this resulted in highly reproducible oxide layers with respect to layer thickness and homogeneity as already demonstrated in our earlier work.[25] The first (galvanostatic) stage of anodization is characterized by a constant current flow until the potential reaches the desired voltage of formation. During the second stage (potentiostatic) the potential (40 V) is fixed for the desired anodization time (180 min) while the current flow decays. Oxidation is performed in a polycarbonate oxidation cell using a stainless steel counter electrode, whereas the power supply was realized by a Knürr-Heinzinger PTN 250-2 galvanostat/potentiostat. After anodization and washing in de-ionized water at temperatures between 30 °C and 60 °C, samples were arbitrarily selected to perform electrical and microstructural characterization after this first anodization step. All other samples were subjected to further processing involving (i) annealing at 260 °C or 320 °C for 1 h in air, (ii) annealing at 260 °C or 320 °C for 1 h in air and subsequent re-anodization at 40 V for 60 min. Annealing was performed in a KENDRO UT 6060 oven in air. Additionally, annealing of the anodized samples at 320 °C was also performed in a NETZSCH TG 439 thermobalance in air and nitrogen atmosphere. In order to investigate the influence of different thermal load on the electrical properties and resulting microstructure of the Nb_2O_5/Nb-heterostructure, anodized samples were annealed in the temperature range between 200 °C and 350 °C for 1 h in air in a second series of experiments. A flow chart for the preparation and characterization of samples investigated in this study is given in Fig. 1.

2.2. Electrical characterization

The electrical characterization of both, oxidized and annealed niobium anode samples was performed as a "wet test" in a platinated silver beaker in a liquid electrolyte (18 % H_2SO_4) at 25 °C, utilizing a Zahner IM6 impedance analyzer with a CVB 80 voltage booster. Since the specific conductivity of 18 wt% H_2SO_4 is significant high, any influence of the measuring electrolyte conductivity on capacitance measurements can be excluded.[20] The measurements were performed at $f = 120$ Hz with bias voltages ranging from −0.5 V to 15 V. All measured capacitances $C_{meas.}$ were transformed into specific charge values Q according to $Q = C_{meas} \cdot U_{ox}$. where U_{Ox}. represents the formation voltage (40 V). If the specific charge is normalized with respect to the mass of the capacitor anode m_{Anode}, the mass-specific charge Q/m_{Anode} is obtained which provides a basis for comparison of different samples. The mass-specific charge is denoted commonly as specific capacity within the capacitor fabricating industry. This definition implies that the area of the dielectric layer does not change during processing. This is justified, since annealing temperatures applied in this study are significantly lower than typical sintering temperatures.

2.3. Microstructural characterization

Microstructural characterization of the sintered powder compacts was performed after electrolytic oxide layer formation and subsequent annealing. The overall microstructure and oxide layer thickness of the different samples was determined using a LEO 1530 scanning electron microscope. Detailed microstructural investigations were carried out employing high-resolution transmission electron microscopy (HRTEM) as well as energy-filtered selected area diffraction (SAED), utilizing a Philips CM200FEG/ST (field emission gun) and an energy-filtering Zeiss 912-Omega microscope with 200 kV and 120 kV acceleration voltage, respectively. TEM-foil preparation followed standard techniques, which involve diamond cutting, ultrasound

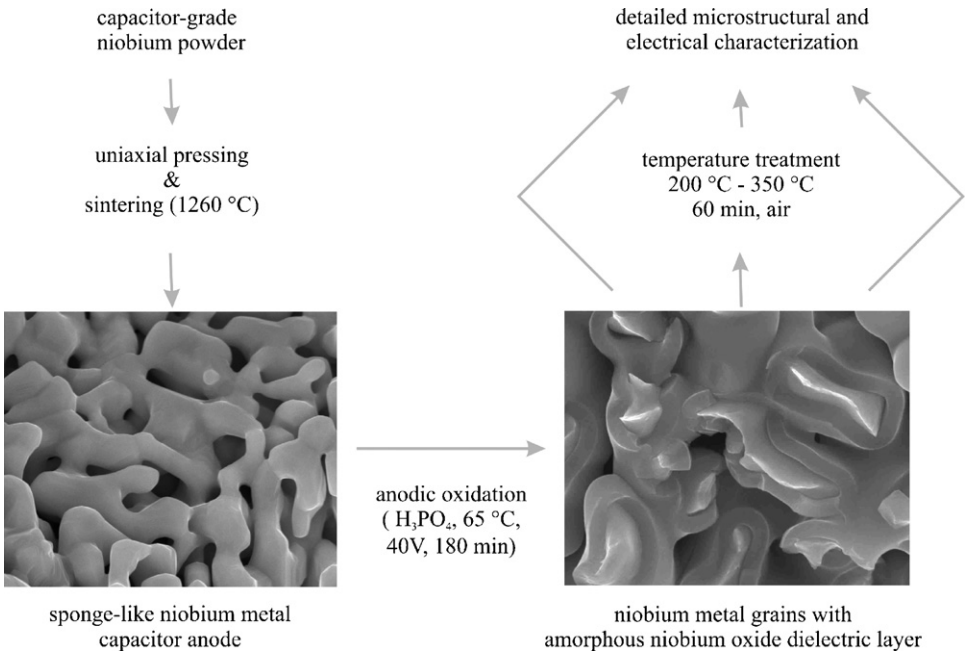

Fig. 1. Flow chart for the preparation and characterization of samples investigated in this study.

drilling, mechanical grinding, dimpling and Ar^+-ion thinning to perforation.

3. Results and discussion

3.1. Influence of anodization and annealing on microstructure and electrical parameters

3.1.1. Bias-dependence of mass-specific charge Q/m_{Anode}

Measurements of Q/m_{Anode} as a function of bias voltage (−0.5–15 V) were performed after (i) first anodization, (ii) annealing at 260 °C/1 h or 320 °C/1 h and after (iii) second anodization. Fig. 2 shows the values of specific capacitance of niobium anodes after these processing steps, determined at a fixed frequency of 120 Hz, as a function of applied DC bias voltage.

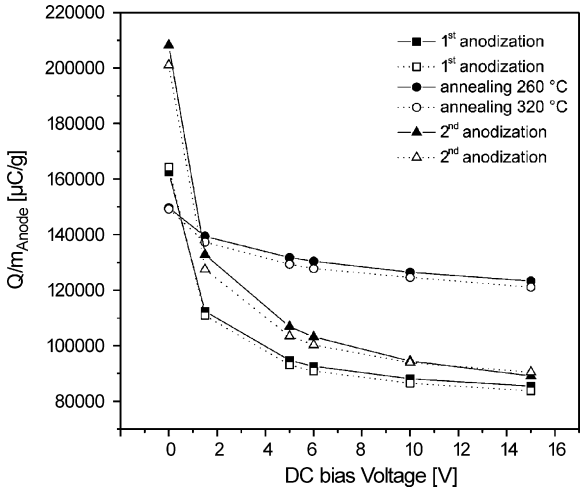

Fig. 2. DC bias voltage dependent capacitance of niobium anodes after (i) first anodization (squares), (ii) annealing at 260 °C (solid circle) or 320 °C (open circle) for 1 h in air as well as after (iii) re-anodization (triangles).

The electrical measurements reveal a large bias dependence of Q/m_{Anode} after the first anodization. The values of Q/m_{Anode} decrease from approximately 160,000 µC/g at 0 V bias voltage to 80,000 µC/g, at a 15 V DC bias. This bias-dependence of specific capacitance after anodization cannot be found for the Ta/Ta_2O_5-capacitors, which demonstrates a characteristic difference between the two material systems. Annealing of the Nb-capacitor samples after anodization results in a markedly reduced bias dependence of Q/m_{Anode}. In this case, only a slight decrease from 150,000 µC/g (0 V DC bias) to 130,000 µC/g (15 V DC bias) is observed. It has to be noted, that the annealing temperature showed no detectable influence on the bias dependence and electrical response of the niobium capacitor anodes, resulting in the same specific capacitance values for samples annealed at 260 °C or 320 °C, respectively. Finally, the second anodization step after thermal treatment of the samples again strongly enhances the bias dependence of Q/m_{Anode}. High values up to 210,000 µC/g are determined at 0 V bias, whereas Q/m_{Anode} at 15 V DC bias voltage is in good agreement with the values after first anodization. Also, an influence of the temperature of the preceding annealing step cannot be detected. The measured values of Q/m_{Anode} for samples annealed at 260 °C (solid triangle) as well as for samples annealed at 320 °C (empty triangle) are in very good agreement. Moreover, the effect of large bias dependence of the specific capacitance after anodization and *vanishing* bias dependence of the specific capacitance after thermal treatment is completely *reversible* and can be repeated several times without noticeable change of the already discussed behavior.[26] Multiple anodization and thermal annealing procedures at 320 °C for 1 h always results in the same behavior with respect to the bias dependence of Q/m_{Anode}.

The bias dependence of Q/m_{Anode} after oxide layer formation within Nb-anodes was also reported by Schnitter et al.[10] and Stenzel et al.[27] It can be explained by a n-type semiconducting behavior of the anodically formed oxide layer. In contrast to the Ta/Ta_2O_5 system where a steep oxygen gradient is expected at the interface because Ta_2O_5 is the only stable oxide phase within the tantalum-oxygen system, the niobium oxygen system is much more complex. Niobium occurs in various oxidation states, resulting in a variety of stable Nb-oxides (NbO, NbO_2, Nb_2O_5) with a wide range of electrical properties ranging from metallic conductivity (NbO) to dielectric for stoichiometric Nb_2O_5. Besides the stoichiometric Nb_2O_5, different oxygen-deficient metastable niobium pentoxide phases Nb_2O_{5-y} exist which exhibit n-type semiconducting behavior.[28] Since the anodization of Nb involves not only the transport of niobium cations from the anode through the oxide layer towards the oxide–electrolyte interface, but also the migration of oxygen ions towards the Nb_2O_5/Nb-interface, it is therefore plausible that residual oxygen vacancies exist within Nb_2O_5 layer. Hence, anodically formed Nb_2O_5 films contain a significant donor density in the space-charge layer below the surface oxide indicating n-type semiconducting behavior.[29,30] Additionally, several authors reported on the formation of thin layers of different niobium-oxide phases at the metal-dielectric oxide interface.[31,32] The existence of the oxygen vacancies accumulated at the metal–oxide interface was clearly demonstrated by Kovács et al.[33]. Therefore, the observed bias dependence of Q/m_{Anode} of Nb-anodes after anodization can be explained by the existence of n-type semiconducting regions within the oxide layer. Due to these semiconducting properties of the O-deficient Nb_2O_5 region near the metal–oxide interface, a Schottky diode configuration is obtained. This causes the formation of a space charge region within the oxide layer and thus induces the bias dependence of Q/m_{Anode} since the Fermi levels of Nb and the Nb_2O_5 layer near the metal interface are aligned.[10]

Annealing of niobium anodes results in the aforementioned reduction of bias dependence of specific capacitance, hence indicating a decreasing vacancy concentration. This is accompanied by the formation of stoichiometric niobium pentoxide due to recombination of the oxygen vacancies with oxygen from the ambient annealing atmosphere nearby the niobiumoxide–atmosphere interface upon heat treatment (see also Section 3.3). The assumption of decreasing O-vacancy concentrations upon annealing of the capacitor anodes at 260 °C or 320 °C/1 h was confirmed by an analysis of the electrical measurements on the basis of the Mott-Schottky equation.[34,35] This analysis resulted in calculated donor densities ranging from $8 \times 10^{18}/cm^3$ for as-anodized samples to $2 \times 10^{18}/cm^3$ for oxidized and annealed samples.[36]

The described electrical response of as-anodized and annealed niobium anode capacitor samples is in contrast with the early work of Smyth et al.[20,37–40] who examined the effect of elevated temperatures on the electrical performance of the Ta/Ta_2O_5- and Nb/Nb_2O_5-systems in detail. During their comprehensive studies they were able to demonstrate that the temperature dependence of the capacitance of as-formed Nb_2O_5 films is much higher than for the comparable tantalum

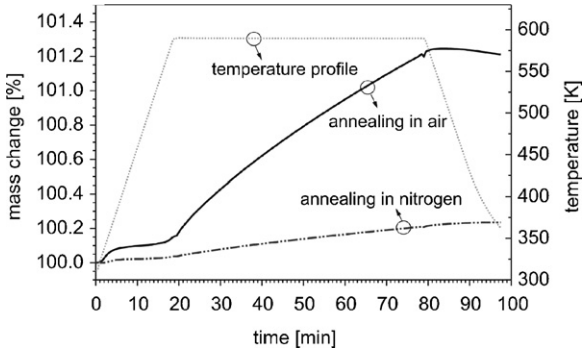

Fig. 3. Thermal annealing of oxidized niobium anodes in a thermobalance provides evidence for strong oxygen uptake during annealing in air as indicated by the mass increase of the niobium samples (solid line). In contrast to annealing in air, mass increase upon annealing in nitrogen atmosphere is negligible (dashed line).

case. Since this temperature dependence of capacitance can be attributed to thermal activation of charge carriers, a large DC bias dependence of capacitance would be expected in annealed samples.

After annealing treatment of as-anodized Ta-capacitor samples above 200 °C in air, Smyth et al. were able to show that, an O-depleted layer near the metal–metal oxide interface is formed within the Ta_2O_5 layer resulting in a strong bias, frequency and temperature dependence of dielectric properties. According to Smyth et al., the Nb/Nb_2O_5-system behaves more sensitively to thermal treatment compared to the Ta/Ta_2O_5-system but in principle in the same manner with respect to the aforementioned O-depletion layer. In our study, however, annealing of the Nb/Nb_2O_5-samples results in a reduction of the Q/m_{Anode} bias dependence. One possible explanation of these contrary results might be due to thermally induced physical damage within the samples investigated by Smyth et al. since in ref. [20] it was mentioned that physical damage might be localized at the edge of the samples. Moreover, capacitor-grade niobium powders were not available that time.

3.1.2. Annealing in the thermobalance

Thermogravimetric analyses of the annealing was performed in a thermobalance under conditions similar to the annealing step in the furnace. Fig. 3 reveals a remarkable mass increase of as-anodized Nb-anodes of up to 1.2% for annealing at 320 °C. The mass increase is strongly reduced (<0.2%) if the annealing is performed in a nitrogen atmosphere. The small mass increase in the latter case can be assigned to oxygen incorporation due to residual oxygen in the annealing atmosphere.

In contrast to the Nb-anodes, oxidized Ta-anodes or stoichiometric crystalline Nb_2O_5 powder only show negligible mass increase upon heat treatment in air. It is concluded that annealing of the anodized Nb-anodes in air leads to a significant oxygen uptake. It is assumed that this excess oxygen is not only incorporated into the Nb-anode but also in the dielectric niobium oxide layer. These results are consistent with the measured reduced donor densities after annealing[36] and support our explanation for the bias dependence of Q/m_{Anode}.

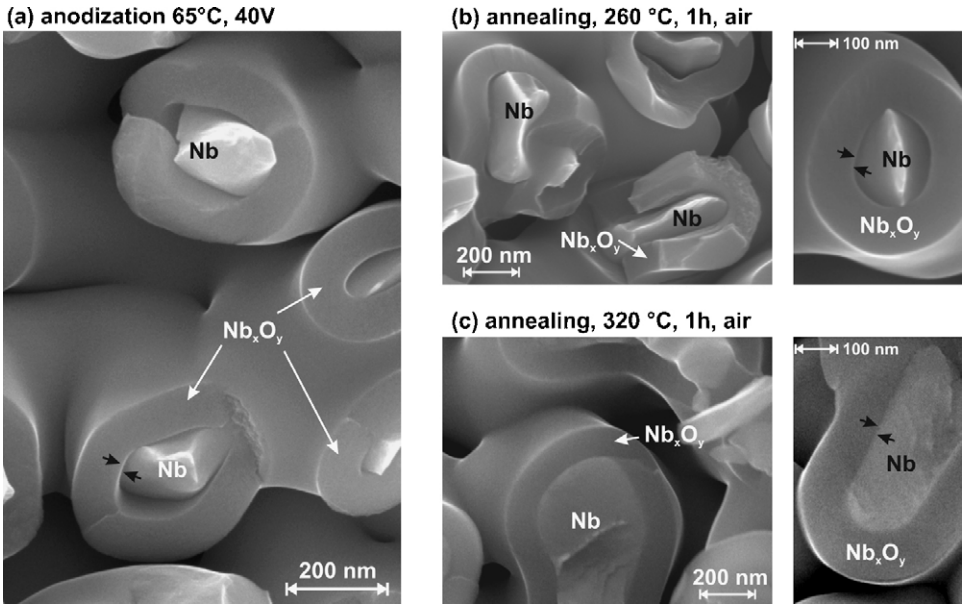

Fig. 4. SEM micrographs of fracture surfaces of niobium anodes after anodization (a) and after annealing at 260 °C (b) or 320 °C (c) for 1 h in air. Annealing at 260 °C does not alter the fracture behavior at the niobium–niobium oxide interface of the samples which is characterized by a clearly visible interface region (black arrows in (a) and (b)). After annealing at 320 °C/1 h/air remarkable changes at the metal–metal oxide interface can be visualized (black arrows in (c)), indicating structural changes at the niobium metal–niobium oxide interface upon heat treatment exceeding 300 °C.

3.1.3. Microstructural characterization by means of SEM

SEM micrographs of fracture surfaces are presented in Fig. 4 after anodization (a), annealing at 260 °C/60 min (b) and annealing at 320 °C/60 min (c). The fracture surface between Nb-anode and the amorphous Nb_2O_5 is characterized by a clearly observable interface after anodic oxidation (Fig. 4(a)) and annealing at 260 °C (Fig. 4(b)). A remarkable change of the fracture behavior is observed after annealing at 320 °C (Fig. 4(c)). In this case, the interface between niobium metal and amorphous niobium oxide is smooth, indicating microstructural changes at the interface and/or possibly pronounced oxygen diffusion across the interface during high temperature annealing.

The average oxide-layer thickness was also determined by means of SEM investigations. Table 1(a) shows the determined oxide thickness values after the different processing steps with the corresponding values for Q/m_{Anode} at 10 V DC bias voltage. It is noted, that every mean value of the oxide-layer thickness in Table 1 corresponds to 50 individual measurements covering different grains. The average Nb_2O_5-layer thickness is not altered after annealing and second anodization despite of significant changes for Q/m_{Anode}. Hence, the thickness measurements show that thickness changes of the Nb_2O_5-layer cannot be the origin of the capacitance change.

In Table 1(b) mean oxide-layer thicknesses of individual samples are given which were anodized under identical conditions (1 wt% H_3PO_4, 65 °C, 40 V, 180 min) in consecutive batches. Those values vary only between 126.8 nm and 128.4 nm, demonstrating the good reproducibility of the anodization process.

3.1.4. Microstructural characterization by means of TEM

HRTEM investigations were performed to clarify whether structural changes are observed in the amorphous Nb_2O_5-layer or at the Nb/Nb_2O_5-interface after different processing steps which could be related to oxygen uptake during high temperature annealing or formation of an oxygen depleted region near the Nb/Nb_2O_5-interface due to oxygen extraction from Nb_2O_5

Table 1
Mean values of niobium oxide layer thickness after various processing steps as determined employing SEM as well as corresponding values of mass-specific charge Q/m_{Anode} determined with 10 V DC bias (a). Each mean oxide layer thickness value corresponds to 50 individual measurements of the oxide layer covering different niobium metal grains. The determination of oxide layer thickness values of different as-anodized samples which were anodized in consecutive batches under equal anodization conditions demonstrate the good reproducibility of the phosphoric acid anodization process (b).

Part (a)

	1st oxidation, 1% H_3PO_4, 65 °C 40 V/180 min	1st annealing, 260 °C/60min, air	2nd oxidation, 1% H_3PO_4, 65 °C 40 V/60 min
Layer thickness [nm]	127.9 ± 0.8	127.6 ± 0.7	127.6 ± 0.7
Mass-specific charge [μC/g]	88,000	123,000	94,000

Part (b)

1st oxidation, 1% H_3PO_4/65 °C 40 V/180 min	sample 1	sample 2	sample 3	sample 4	sample 5
Oxide layer thickness [nm]	127.6 ± 0.7	127.9 ± 0.8	128.4 ± 0.5	126.8 ± 0.7	127.1 ± 0.9

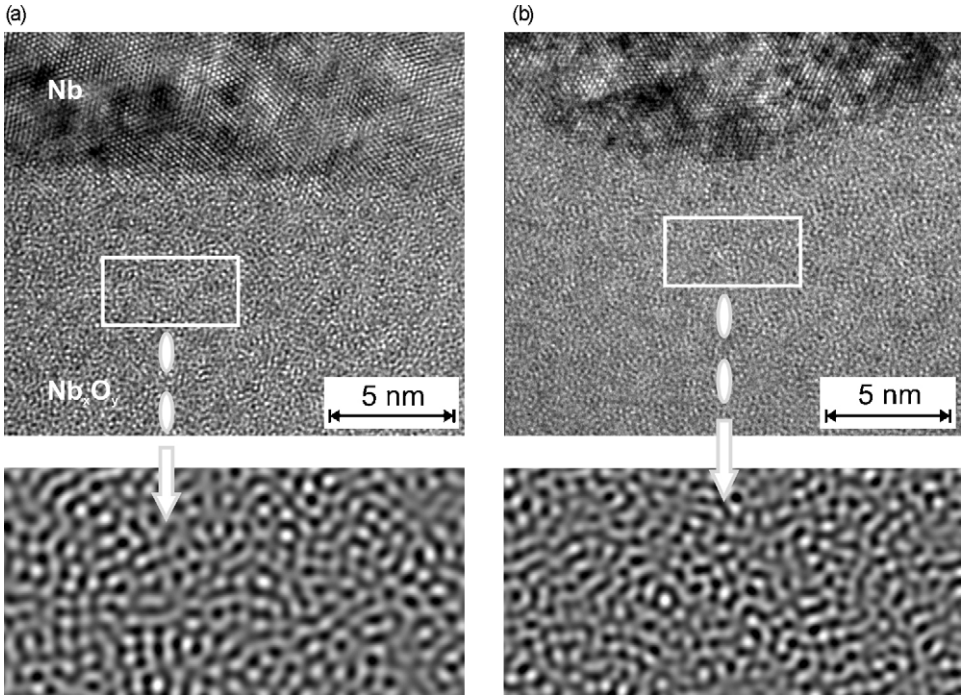

Fig. 5. HRTEM micrographs of the interface region niobium metal–niobium oxide layer after anodization (a) and subsequent thermal treatment at 320 °C for 1 h in air. HRTEM investigations gave no evidence for structural alteration and/or crystallization phenomena within the amorphous dielectric oxide layer.

by the niobium grain.[9,21,24] HRTEM images of the interface region before and after high-temperature annealing are shown in Fig. 5(a) and (b), respectively.

A sharp interface is observed between the crystalline Nb-grain and the adjacent amorphous Nb_2O_5-layer after anodization (Fig. 5(a)). There is no indication for the formation of a strongly "oxygen-depleted" region consisting of NbO or NbO_2 between Nb and Nb_2O_5. Additional investigations by means of electron energy loss spectroscopy (EELS) across the interface region revealed, that the transition between metal anode and amorphous Nb_2O_5 takes place within a few nanometers.[41] Annealing at 320 °C/1 h in air (Fig. 5(b)), does not lead to structural alterations which are detectable by HRTEM. Additional Fourier-filtering of the HRTEM images in the amorphous layer region adjacent to the Nb-grain (Fig. 5(a) and (b) bottom) did not yield any indication for phase separation or nucleation of crystalline phases.

This finding is in contrast to earlier investigations by Pozdeev-Freeman[23] or Olszta[42] who reported on the temperature- or field-induced crystallization of anodically formed Nb_2O_5. However, one has to consider carefully the preparation conditions of the amorphous Nb_2O_5-film since the crystallization rate depends on many factors including (i) anode purity and surface area, (ii) temperature and concentration of anodization electrolyte (iii) anodization voltage and anodization time as well as (iv) post-formation thermal treatment. Since the crystallization rate is thought to increase with increasing thickness of the oxide film, it is reasonable that the approximately 130 nm thick Nb_2O_5 layers in this study withstand field-induced crystallization upon formation.

In addition to HRTEM, energy-filtered SAED was performed to detect possible stoichiometry variations due to annealing which could induce changes of the short-range order (nearest neighbor distances). Fig. 6 shows the radial intensity distribution obtained on the basis of the SAED patterns as a function of the spatial frequency u before (a) and after (b) annealing at 320 °C. The extracted values for the nearest-neighbor distances are given by 1/u at the maxima of the radial intensity distribution (Table 2). The radial intensity distributions were obtained by rotationally averaging the intensity of the SAED patterns. Those as-received raw data were background subtracted with a second-order exponential decay function and a Gaussian multi-peak fitting procedure was applied to determine the position of the peak maxima.

Table 2 and Fig. 6 show that annealing does not alter the overall structural properties of the amorphous oxide layer within the achievable accuracy of this technique. In all cases, nearest-neighbor distances of 0.34 nm, 0.26 nm and 0.17 nm are compatible with the Nb_2O_5 phase. Consequently, severe composition changes of the amorphous oxide layer can be excluded up to annealing temperatures of 320 °C. However, we note that only the structural assembly of the amorphous Nb_2O_5 averaged over a sample area with a diameter of 100 nm was analyzed. Recent quantitative EELS investigations with high spatial resolution indicate a measurable oxygen deficiency at the Nb/Nb_2O_5 interface after high-temperature annealing. These measurements are based on elaborate sensitivity-factor determination in the Nb/O-system and will be presented in a separate study.[43]

3.2. *Influence of the annealing temperature on Q/m_{Anode} and microstructure*

To investigate the impact of annealing on Q/m_{Anode} and the resulting microstructure, the annealing temperature was varied between 200 °C and 350 °C in a second series of experiments.

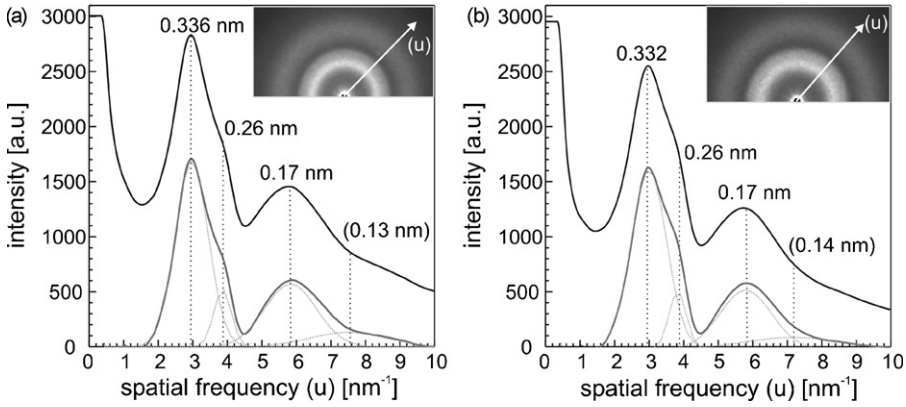

Fig. 6. Radial intensity distributions of the SAED patterns (insets top right corners) after anodization (a) and after subsequent annealing at 320 °C/1 h/air (b). The evaluated nearest neighbor distances are the same in all samples investigated, hence indicating no major microstructure rearrangements or changes in stoichiometry within the amorphous niobium oxide layer upon temperature treatment.

Table 2
Evaluated nearest neighbor distances within the amorphous niobium oxide layer after anodization (a) and subsequent annealing at 320 °C for 1 h in air (b).

SAED pattern #	(a) After anodization			(b) After annealing 320 °C, 1 h, air		
	d_1	d_2	d_3	d_1	d_2	d_3
1	0.335	0.263	0.170	0.330	0.261	0.174
2	0.339	0.261	0.169	0.335	0.261	0.168
3	0.337	0.262	0.173	0.332	0.261	0.173
4	0.337	0.260	0.169	0.333	0.262	0.174
5	0.338	0.261	0.169	0.336	0.261	0.173
6	0.339	0.261	0.169	0.332	0.261	0.168
7	0.337	0.260	0.173	0.331	0.260	0.173
8	0.335	0.261	0.169	0.334	0.262	0.171
Mean value [nm]	0.337 ± 0.002	0.261 ± 0.001	0.170 ± 0.002	0.333 ± 0.002	0.261 ± 0.001	0.172 ± 0.002

The annealing was carried out for 1 h in air. The measured Q/m_{Anode} values are listed in Table 3. All Q/m_{Anode} values were determined at 10 V DC bias where the influence of applied bias voltage becomes almost independent of the processing step according to Fig. 2. Due to this fact a general statement regarding the increase or decrease of specific capacitance can be made irrespective of the capacitance which might be reached within such capacitor systems during application.

According to Table 3, Q/m_{Anode} after annealing is always higher compared to the as-anodized sample. However, a maximum value is reached at 300 °C.

Since characterization of the Nb_2O_5 after anodization and annealing at 260 °C or 320 °C did not yield any detectable microstructural changes (see Section 3.1.3), the crystalline Nb-anodes in this sample series were analyzed by SAED. Representative SAED patterns for the as-anodized samples (40 V) and for samples annealed below and above 300 °C are shown in Fig. 7.

Structural changes are observed at annealing temperatures exceeding 300 °C. The SAED patterns of the anode of the as-anodized sample (Fig. 7(a)) and the samples annealed at 250 °C (b) and 300 °C (c) correspond to niobium with space-centered cubic structure along the [111]-zone axis. Superstructure reflections indicating a quadrupling of the lattice parameter can be observed in the SAED pattern after annealing at 320 °C (Fig. 7(d)). This superstructure can be assigned to Nb_6O,[28] which is formed in oxygen-oversaturated niobium. The incorporation of oxygen in Nb-anodes up to the solubility limit was already reported by Pozdeev-Freeman.[44] They detected shifts in X-ray diffractometry patterns towards higher lattice parameters in niobium, indicating oxygen absorption in the metal after powder sintering and further processing at temperatures up to 525 K. It was suggested, that this oxygen incorporation is a gradual process beginning at the first annealing which continues during high-temperature processing until the solubility limit of oxygen in niobium is reached. Our results indicate that oxygen uptake

Table 3
Specific capacitances (measured at f = 120 Hz, U_{Bias} = 10 V) of as-anodized and annealed oxidized niobium anodes. Annealing steps were performed at temperatures between 200 °C and 350 °C for 1 h in air.

1st oxidation [μC/g]	Annealing at 200 °C/1h [μC/g]	Annealing at 250 °C/1h [μC/g]	Annealing at 260 °C/1h [μC/g]	Annealing at 300 °C/1h [μC/g]	Annealing at 320 °C/1h [μC/g]	Annealing at 350 °C/1h [μC/g]
80545 ± 429	95539 ± 526	108302 ± 1136	115261 ± 1104	118216 ± 0	116357 ± 526	93680 ± 0

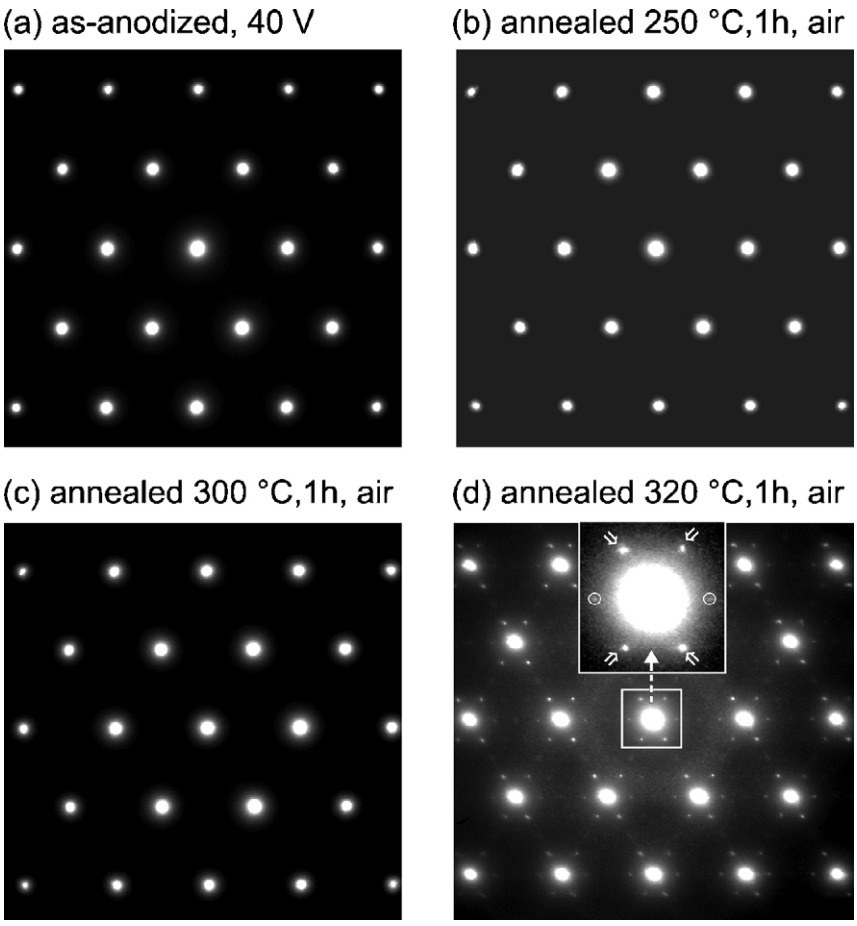

Fig. 7. SAED patterns of arbitrarily selected niobium metal grains within the niobium capacitor samples after anodization (a) and subsequent annealing in air for 1 h at 250 °C (b), 300 °C (c), or 320 °C (d). Whereas the diffraction pattern of the as-anodized sample as well as the samples annealed up to 300 °C reflects the diffraction pattern of a purely bcc niobium metal structure, additional diffraction intensities can be imagined after annealing at 320 °C. These diffraction intensities can be assigned to a Nb_6O superlattice which is formed in oxygen oversaturated niobium metal.

of the anodized niobium capacitor upon annealing as well as oxygen migration towards the Nb-anode is very sensitive to the annealing temperature. Moreover, incorporation of oxygen in niobium is not limited by the solubility limit as shown by the O-induced superlattice reflections in Fig. 7(d) for the samples annealed above 300 °C. We note that annealing at 300 °C for 1 h in air appears to be a critical condition because this is the highest annealing temperature without changes of the fracture behavior at the Nb/Nb_2O_5-interface compared to the as-anodized samples (see Fig. 4 (a)). It also coincides with the maximum Q/m_{Anode} (see Table 3). Annealing above 300 °C is correlated with an oversaturation of the Nb-anode with oxygen as shown by the formation of Nb_6O (Fig. 7(d)) and a change of the fracture surface (see Fig. 4(c)).

It is noted that the effect of phosphorous incorporated in the oxide film during anodization due to the phosphoric acid in electrolyte which was reported by several researchers[45–47] has been neglected so far. This incorporation of a certain amount of phosphorous into the outer part of the Nb_2O_5 layer is thought to have a significant influence on O-kinetics and, hence, on microstructural development and resulting electrical response. Since Ta_2O_5 films on tantalum, anodically grown in diluted sulfuric acid are more nearly stoichiometric and did not show incorporation of electrolyte species,[45] further work will also focus on sulfuric acid as electrolyte for anodization of Nb. First experiments using 0.175 wt.% sulfuric acid as liquid electrolyte show homogeneous Nb_2O_5-layer growth with respect to layer thickness and specific capacitances which are comparable to those presented in the current paper.

3.3. Model for the configuration of the Nb_2O_5 dielectric after different processing steps

The electrical and microstructural properties of Nb-based capacitors after anodization and subsequent thermal annealing presented in this study confirm the frequently cited sensitivity of the Nb/Nb_2O_5-system at elevated temperatures. However, in contrast to earlier investigations, adverse effects on the electrical properties due to inhomogeneities in the Nb-powder or cracks and fissures within the capacitor structure are excluded in this study. In good accordance with earlier investigations[9] it is shown, that Q/m_{Anode} of our capacitors is markedly increased (at 10 V DC bias) after annealing compared to the as-anodized samples although there is no detectable change in dielectric layer thickness nor any indication for remarkable changes (e.g. nucleation/crystallization effects) within the amorphous dielectric

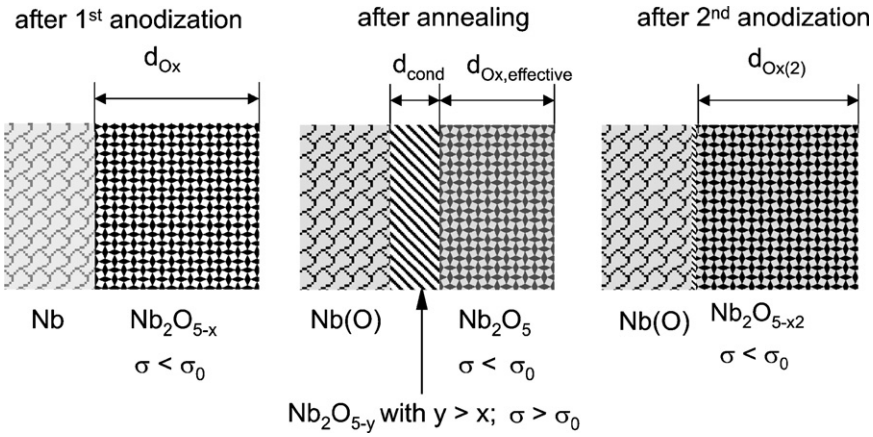

Fig. 8. Model for the interface region niobium metal–niobium oxide layer after anodization (left), annealing (middle), and subsequent re-anodization (right). The oxygen layer is oxygen deficient after formation, exhibiting the composition Nb_2O_{5-x}. During annealing in air, an intermediate conductive layer with a conductivity $\sigma > \sigma_0$ is formed due to oxygen extraction from the dielectric oxide layer by the niobium metal core. Hence, this intermediate layer is resistive and contributes not longer to the capacitance. As a result, the effective dielectric oxide layer thickness is reduced and electrical investigations indicate an increase in capacitance. Moreover, an oxygen uptake from the ambient annealing atmosphere (air) into the oxide layer adjacent to the atmosphere occurs, leading to more stoichiometric niobium oxide within the remaining dielectric oxide layer. During re-anodization, the conductive layer is re-anodized, resulting in a decrease of capacitance due to a larger dielectric layer thickness.

layer. Taking the bias dependence of Q/m_{Anode} into account, the following model for the observed behavior is suggested (Fig. 8).

After the first anodization, a dielectric oxide layer of thickness d_{Ox} (for $V_{ox} = 40$ V, $d_{ox} = 128$ nm) covers homogeneously each individual Nb-grain. This dielectric oxide Nb_2O_{5-x} is not stoichiometric but contains oxygen vacancies which act as donors. Upon annealing, oxygen is extracted by the Nb-anode, which leads to a strongly oxygen-deficient, intermediate layer with high conductivity and a thickness d_{cond} (Fig. 8, "after annealing"). We assume that the intermediate layer does not consist of a certain fixed Nb_2O_{5-y} composition but contains a steep oxygen gradient. However, the oxygen depletion and therefore the conductivity σ in this part of the oxide film exceeds a certain value σ_0 according to Smyth et al.[20] with the result that the electrical response can be described as a purely resistive one and no longer as capacitive. As a consequence, the effective thickness of the dielectric layer $d_{Ox,effective}$ decreases (Fig. 8, "after annealing") which leads to the observed increase of the specific capacitance. Based on the capacitance measurements at $U_{Bias} = 10$ V, a reduction of the effective dielectric thickness of 30% can be assumed (with $C \propto 1/d$), leading to an increase of Q/m_{Anode} of about 44% after thermal annealing at 300 °C. Under the presumption that the area A of the capacitor anode will not change upon processing, $d_{Ox,effective}$ can be estimated to ~89 nm. Hence, the thickness of the conducting intermediate layer can be assumed to be approximately 39 nm. Both layers are completely amorphous as shown in Fig. 5((a) and (b)) and are solely distinguishable by their oxygen-vacancy content.

Possible oxygen diffusion at the Nb_2O_5-surface must also be considered. Based on the thermogravimetry results (Section 3.1.2), which show a mass increase during annealing in air, we conclude that oxygen uptake from the annealing atmosphere into the originally oxygen-deficient Nb_2O_5 must occur. As a result, the donor density and oxygen deficiency in the outer part of the dielectric layer is reduced after annealing and the average composition shifts towards stoichiometric Nb_2O_5 which explains the markedly reduced bias dependence of. Q/m_{Anode} compared to the as-anodized samples. We emphasize that the electrical measurements have to be performed at a 10 V bias to eliminate the bias dependence of Q/m_{Anode}. Oxygen uptake by Nb_2O_5 and oxygen extraction by the Nb anode is more pronounced at annealing temperatures above 300 °C. This leads to the formation of Nb_6O in the anode, the change in fracture behavior at the Nb/Nb_2O_5 interface, the less pronounced increase (reduction with respect to the maximum value at 300 °C) of the mass-specific charge Q/m_{Anode} with respect to the as-anodized sample. Finally, during a second anodization step the conductive intermediate layer d_{cond} is re-oxidized resulting in almost the same dielectric response as after the first anodozation.

The assumption of a conductive intermediate layer after annealing is confirmed by the analysis of the starting phase of the 2nd formation step after annealing (Fig. 9(a)). Fig. 9(b) compares the charging curve of a corresponding ideal capacitor ($U_c(t)$) and the measured formation curve ($U_{F2}(t)$) for the sample annealed at 260 °C. The formation curve of the samples which were exposed to the 2nd formation step without annealing follow the charging curve of the niobium capacitor until the desired formation voltage $U_{F2} = 39$ V is reached. The second formation curves of samples annealed at 260 °C and 320 °C show a strong deviation from the ideal capacitor behavior. After annealing at 260 °C respectively 320 °C the dwell time at a constant current density of 150 mA/g to reach the maximum voltage of 39 V is prolonged. This has to be attributed to an anodic oxidation process occurring after the annealing. According to the deviation between calculated and measured loading curves, the conclusion can be drawn that a conductive intermediate layer, exhibiting a lower oxygen content, is formed during the annealing of niobium capacitor anodes and that this conducting layer is anodically oxidized during the following formation step.

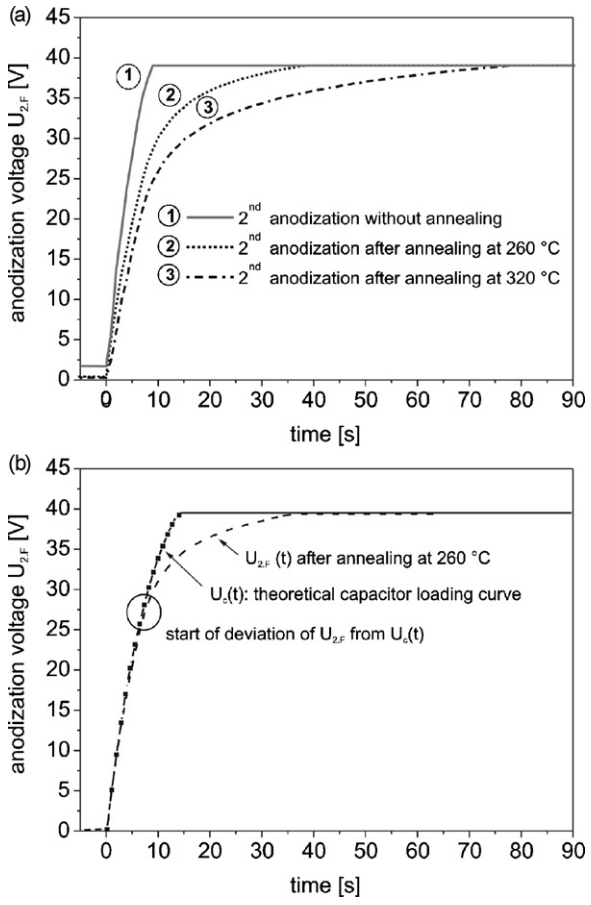

Fig. 9. Anodization voltage vs. time curves of the starting phase of the re-anodization step of the niobium capacitor samples after annealing in air at 260 °C (dotted line), 320 °C (dashed line) as well as without annealing (solid line). The three formation lines differ apparently from each other, supporting the assumption that during annealing an intermediate conductive layer is formed which is re-anodized during the second anodization step. Comparison of the theoretical loading curve of a capacitor (which should correspond to the voltage increase at the beginning of the galvanostatic 2nd formation step) with the anodization voltage vs. time curve of the starting phase of the 2nd formation of the sample that was annealed at 260 °C. Starting at a voltage of approximately 27 V, a deviation between the theoretical loading curve and the anodization vs. time curve of the capacitor can be imagined, supporting the aforementioned assumption of re-oxidation of an intermediate conductive layer.

4. Conclusion

The influence of thermal annealing on the electrical properties and microstructure of oxidized Nb-anodes has been studied using impedance spectroscopy as well as scanning (SEM) and transmission electron microscopy (TEM). The results indicate, that anodically formed Nb_2O_5 layers on niobium contain oxygen vacancies which act as donors resulting in a n-type semiconducting behavior. The capacitance after anodization is strongly bias-voltage dependent which can be explained by a Schottky diode configuration at the Nb_2O_5/Nb-interface. Annealing in air leads to an improved electrical performance by (a) an increase of the capacitance and (b) a reduction of the bias-voltage dependence of the capacitance. Moreover, a remarkable oxygen uptake is observed by thermogravimetric measurements. However, this oxygen uptake is sensitive to the annealing temperature. Annealing in air for 1 h at temperatures up to 300 °C predominantly causes the oxygen to be dissolved in the oxygen-deficient Nb_2O_5 layer close to the surface and results in an improved dielectric performance. Annealing also induces oxygen diffusion from the Nb_2O_5 into the Nb-anode which leads to the formation of a thin, conductive intermediate niobium-oxide layer. But this extraction of oxygen from the dielectric layer is of minor peculiarity when compared to the overall oxygen uptake into the capacitor sample, hence resulting in markedly improved electrical performance after annealing. Annealing at temperatures above 300 °C for 1 h in air is characterized by a strong oxygen migration into the Nb-anode. The uptake of oxygen in Nb is not limited to the solubility limit of oxygen in niobium as established by SAED investigations of the Nb-anode of samples annealed at 320 °C. An O-induced superstructure consistent with Nb_6O is detected which is only formed in oxygen-oversaturated niobium. A second anodization step after annealing again leads to a strong bias dependence of the capacitance. We conclude that annealing treatments improve the electrical performance of Nb-based capacitors by (a) improving the dielectric properties of the oxygen-deficient Nb_2O_5 and (c) increasing the capacitance due to the reduced effective thickness of the dielectric layer.

Acknowledgments

The authors thank the Bundesministerium für Bildung und Forschung (BMBF) for financial support throughout the work. We are grateful to Dr. Stenzel and Dr. Zillgen, EPCOS AG, Heidenheim for fruitful discussion and for providing some of the samples investigated in this study.

References

1. Lohwasser, W., Knabe, W. and Gerblinger, J., Processing and testing of high-cap tantalum capacitors. In *Proceedings of the 19th Passive Components Symposium (CARTS USA)*, 1999, pp. 308–313.
2. Kobayashi, A., Nishiyama, T., Nakata, T., Morimoto, K. and Watanabe, K., The history and future development of tantalum capacitors. In *Proceedings of the 10th Passive Components Symposium (CARTS Europe)*, 1996, p. 49.
3. Edson, D. and Wadler, D., A new low ESR fused solid tantalum capacitor. In *Proceedings of the 26th Passive Components Symposium (CARTS USA)*, 2006, pp. 281–290.
4. Hahn, R., Piller, J. and Lessner, P., Improved SMT performance of tantalum conductive polymer capacitors with very low ESR. In *Proceedings of the 26th Passive Components Symposium (CARTS USA)*, 2006, pp. 291–303.
5. Dias, D., Carvalho, P. A., Ferro, A. C., Monteiro, P. and Lohwasser, W., ESR improvement of Ta capacitors by optimisation of cathode formation. In *Proceedings of the 19th Passive Components Symposium (CARTS Europe)*, 2005, pp. 17–29.
6. Shtasel, A. and Knight, H. T., An investigation of columbium as an electrolytic capacitor metal. *J. Electrochem. Soc.*, 1961, **108**, 343–347.
7. Schwartz, N., Gresh, M. and Karlik, S., Niobium solid electrolytic capacitors. *J. Electrochem. Soc.*, 1961, **108**, 750–758.
8. Ling, H. W. and Kolski, T. L., Niobium solid electrolyte capacitors. *J. Electrochem. Soc.*, 1962, **109**, 69–70.
9. Qiu, Y., Kitchell, R., Smyth, D. and Kimmel, J., A novel substrate for solid electrolytic capacitors. In *Proceedings of the 21th Passive Components Symposium (CARTS USA)*, 2001, pp. 99–103.
10. Schnitter, C., Michaelis, A. and Merker, U., New niobium based materials for solid electrolyte capacitors. In *Proceedings of the 22th Passive Components Symposium (CARTS USA)*, 2002, pp. 15–20.

11. Beck, K. and Seyeda, H., Tuning the properties of tantalum- and niobium oxides; A key to tailor-made materials for passive components. In *Proceedings of the 17th Passive Components Symposium (CARTS Europe)*, 2003, pp. 217–222.
12. Serjak, W. A., Shekhter, L., Tripp, T. B., Lanin, L. L., Reichert, K., Thomas, O. *et al.*, A new dielectric material for capacitors: niobium. In *Proceedings of the 20th Passive Components Symposium (CARTS USA)*, 2000, pp. 82–85.
13. Fife, J. A., *et al.*, U.S. Patent No. 6,165,623, 2000.
14. Shekter, L. N., *et al.*, U.S. Patent No. 6,171,363, 2001.
15. Zillgen, H., Stenzel, M. and Lohwasser, W., New niobium capacitors with stable electrical parameters. *Active & Passive Electronic Components*, 2002, **25**, 147–150.
16. Zednicek, T., Pelcak, J., Vrana, B., Sita, Z., Millmann, W. A. and Gill, J., Tantalum and niobium technology overview. In *Proceedings of the 16th Passive Components Symposium (CARTS Europe)*, 2002, pp. 97–101.
17. Zednicek, T., Zednicek, S., Sita, Z., McCracken, C., Millman, W. A. and Gill, J., Niobium oxide technology roadmap. In *Proceedings of the 16th Passive Components Symposium (CARTS Europe)*, 2002, pp. 11–14.
18. Zednicek, S., Horacek, I., Zednicek, T., Sita, Z., McCracken, C. and Millman, W., Extended range NbO capacitors through technology and materials enhancements. In *Proceedings of the 19th Passive Components Symposium (CARTS Europe)*, 2005, pp. 57–63.
19. Zednicek, S., Sita, Z., Zednicek, T., McCracken, C. and Millman, W. A., Low ESR and low profile technology on niobium oxide. In *Proceedings of the 17th Passive Components Symposium (CARTS Europe)*, 2003, pp. 187–195.
20. Smyth, D. M. and Tripp, T. B., The heat-treatment of anodic oxide films on niobium. *J. Electrochem. Soc.*, 1966, **113**, 1048–1052.
21. Boiko, B. T., Kopach, V. R., Meletjev, S. M., Pancheha, P. A., Pozdeev, Y. L. and Starikov, V. V., Comparison of the degradation modes in sandwich structures including amorphous oxides of niobium and tantalum. *Thin Solid Films*, 1993, **229**, 207–215.
22. Tripp, T. B., The effects of thermal treatment on the dielectric properties of anodic oxide films on tantalum and niobium A: oxygen migration. In *Proceedings of the 23th Passive Components Symposium (CARTS USA)*, 2003, pp. 21–28.
23. Pozdeev-Freeman, Y. and Gladkikh, A., The effects of thermal treatment on the dielectric properties of anodic oxide films on tantalum and niobium B: crystallization. In *Proceedings of the 23th Passive Components Symposium (CARTS USA)*, 2003, p. 29.
24. Qiu, Y., Smyth, D. and Kimmel, J., The stabilization of niobium-based electrolyte capacitors. In *Proceedings of the 21th Passive Components Symposium (CARTS USA)*, 2001, pp. 169–174.
25. Störmer, H., Ivers-Tiffée, E., Schnitter, C. and Gerthsen, D., Microstructure and dielectric properties of nanoscale oxide layers on sintered capacitor-grade niobium and V-doped niobium powder compacts. *Int. J. Mat. Res.*, 2006, **97**, 794–801.
26. Fischer, V., Weber, A., Krügel, A., Stenzel, M., Zillgen, H. and Ivers-Tiffée, E., Nanoscale anodic oxide layers for new niobium capacitors: electrical and structural properties. In *Proceedings of the 202nd annual Meeting of the Electrochem Soc*, 2002, pp. 78–87.
27. Stenzel, M., Zillgen, H., Kovács, K. and Kiss, G., DC bias voltage dependence of the capacitance of anodized niobium. In *Proceedings of the 23th Passive Components Symposium (CARTS USA)*, 2003, pp. 43–46.
28. Gmelins Handbuch der Anorganischen Chemie, **Vol. 49/B1**, Verlag Chemie, 1970.
29. Heusler, K. E. and Schulze, M., Electron-transfer reactions at semiconducting anodic niobium oxide films. *Electrochimica Acta*, 1975, **20**, 237–244.
30. Sikula, J., Hlavka, J., Sedlakova, V., Grmela, L., Hoeschl, P., Zednicek, T. *et al.*, Conductivity mechanisms and breakdown characteristics of niobium oxide capacitors. In *Proceedings of the 17th Passive Components Symposium (CARTS Europe)*, 2003, pp. 281–285.
31. Gray, K. E., ISS depth profile analysis of anodized niobium. *Appl. Phys. Lett.*, 1975, **27**, 462–464.
32. Darlinski, A. and Halbritter, J., Angle-resolved XPS studies of oxides at NbN, NbC, and Nb surfaces. *Surface Interface Anal.*, 1987, **10**, 223–237.
33. Kovács, K., Kiss, G., Stenzel, M. and Zillgen, H., Anodic oxidation of niobium sheets and porous bodies: heat-treatment of the Nb/Nb-oxide system. *J. Electrochem. Soc.*, 2003, **150**, B361–B366.
34. Biaggio, S. R., Bocci, N., Rocha-Filho, R. C. and Varela, F. E., Electrochemical characterization of thin passive films on Nb electrodes in H_3PO_4 solutions. *J. Braz. Cham. Soc.*, 1997, **8**, 615–620.
35. Stützle, D. and Heusler, K. E., Halbleitereigenschaften anodisch erzeugter Oxidschichten auf Niob. *Z. Physikalische Chemie*, 1969, **65**, 201–215.
36. Fischer, V., Nanoskalige Nioboxidschichten für den Einsatz in hochkapazitiven Niob-Elektrolytkondensatoren, Ph.D. Thesis, Institut für Werkstoffe der Elektrotechnik, University of Karlsruhe, 2005, in german.
37. Smyth, D. M., Shirn, G. A. and Tripp, T. B., Heat-treatment of anodic oxide films on tantalum, I: the effects on dielectric properties. *J. Electrochem. Soc.*, 1963, **110**, 1264–1271.
38. Smyth, D. M. and Tripp, T. B., Heat-treatment of anodic oxide films on tantalum, II: temperature dependence of capacitance. *J. Electrochem. Soc.*, 1963, **110**, 1271–1276.
39. Smyth, D. M., Shirn, G. A. and Tripp, T. B., Heat-treatment of anodic oxide films on tantalum, III: the conductivity profile. *J. Electrochem. Soc.*, 1964, **111**, 1331–1336.
40. Smyth, D. M., Shirn, G. A. and Tripp, T. B., Heat-treatment of anodic oxide films on tantalum, IV: anodization in phosphoric acid solutions. *J. Electrochem. Soc.*, 1966, **113**, 100–104.
41. Bach, D., Störmer, H., Schneider, R., Gerthsen, D. and Sigle, W., EELS investigations of reference niobium oxides and anodically grown niobium oxide layers. *Microsc. Microanal.*, 2007, **13**(Suppl. S02), 1274–1275.
42. Olszta, M., Sloppy, J., Li, J. and Dickey, E. C., Field-induced crystallization of anodized Nb and NbO electrolytic capacitors. *Microsc. Microanal.*, 2007, **13**(Suppl. S02), 810–811.
43. Bach, D., EELS investigations of reference niobium oxides and niobium-based capacitors, Ph.D. Thesis, Laboratorium für Elektronenmikroskopie, University of Karlsruhe, 2008.
44. Pozdeev-Freeman, Y., Niobium capacitors: from raw materials to finished parts. In *Proceedings of the 16th Passive Components Symposium (CARTS Europe)*, 2002, pp. 19–25.
45. Randall Jr., J. J., Bernard, W. J. and Wilkinson, R. R., A radiotracer study of the composition and properties of anodic oxide films on tantalum and niobium. *Electrochimica Acta*, 1965, **10**, 183–201.
46. Cavigliasso, G. E., Esplandiu, M. J. and Macagno, V. A., Influence of the forming electrolyte on the electrical properties of tantalum and niobium oxide films: an EIS comparatrive study. *J. Appl. Electrochem.*, 1998, **28**, 1213–1219.
47. Li, Y.-M. and Young, L., Niobium anodic oxide films: effect of incorporated electrolyte species on DC and AC ionic current. *J. Electochem. Soc.*, 2000, **147**, 1344–1348.